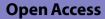## RESEARCH

ADAMTS9-AS1 inhibits tumor growth and drug resistance in clear cell renal cell carcinoma via recruiting HuR to enhance ADAMTS9 mRNA stability

Enyang Zhao[1†], Bo Geng[1†], Ran Tao[3], Bosen You[1], Yunli Liu[1], Wenbin Hou[1], Wanhui Wang[1], Changlin Wang[2*] and Xuedong Li[1*]

[†]Enyang Zhao and Bo Geng contributed equally to this work.

*Correspondence:
wangchanglin1983@126.com;
13604803553@163.com

[1] Department of Urology Surgery, The Second Clinical College, Harbin Medical University, Harbin 150069, Heilongjiang Province, China
[2] Department of Urology, the Fourth Hospital of Harbin Medical University, Yiyuan Street NO.37, Harbin 150001, Heilongjiang Province, China
[3] Department of Urology Surgery, Shenzhen Luohu People's Hospital, Shenzhen 518000, Guangdong Province, China

Abstract

The lack of efficacious treatments for clear cell renal cell carcinoma (ccRCC) has led to a poor 5-year survival rate. Here, we found that the expression of ADAM metallopeptidase with thrombospondin type 1 motif 9 (ADAMTS9) antisense RNA 1 (ADAMTS9-AS1) is commonly decreased in ccRCC tissues. Decreased ADAMTS9-AS1 is associated with advanced stages and poor prognosis in ccRCC patients. Additionally, we found that promoter hypermethylation contributes to the suppression of ADAMTS9-AS1 expression in ccRCC that contained relatively low levels of ADAMTS9-AS1. Further functional studies demonstrated that ADAMTS9-AS1 inhibits cell growth and drug resistance through enhancing mRNA stability of ADAMTS9 in ccRCC. Mechanistically, ADAMTS9-AS1 directly bound to Human Antigen R (HuR). Then, the ADAMTS9-AS1-HuR complex was guided to the ADAMTS9 3'UTR through specific RNA–RNA interaction. Moreover, ADAMTS9-AS1 expression is positively correlated with ADAMTS9 expression in ccRCC tissues. In summary, our data not only highlight the important role of ADAMTS9-AS1 in ccRCC progression, but also reveal new regulatory mechanisms of ADAMTS9, which provides important insights into novel treatment strategies targeting ADAMTS9-AS1-HuR- ADAMTS9 axis in ccRCC.

Keywords: ADAMTS9-AS1, ADAMTS9, HuR, ccRCC, Cell growth

Introduction

Renal cell carcinoma (RCC) is the second most common contributor to mortality in patients with urologic tumors and accounts for approximately 3% of adult malignancies (Ricketts, et al. 2016). Approximately 80–90% of RCCs are clear cell renal cell carcinomas (ccRCCs), which are derived from epithelial cells of the proximal renal tubule and are associated with high metastasis and relapse rates compared with other RCC subtypes (Jonasch et al. 2014). For patients with early stage, localized ccRCC, surgery remains the only possible curative therapy (Hsieh et al. 2017). Nevertheless, approximately one-third

of patients are diagnosed with distal metastasis, and up to 30% of patients relapse after potentially curative surgery (Znaor et al. 2015). The 5-year survival rate of nonmetastatic patients is estimated to be approximately 55%, while that of metastatic patients is only 10% (Posadas et al. 2017; Capitanio et al. 2019). ccRCC, especially advanced and metastatic disease, is resistant to both chemotherapy and radiotherapy and there is currently a lack of effective alternative treatment options (Marconi et al. 2016). Therefore, it is necessary to identify new sensitive, effective early prognostic markers and therapeutic targets for ccRCC.

Long noncoding RNAs (lncRNAs) are a newly discovered class of noncoding RNAs (ncRNAs) that are longer than 200 nucleotides and are not translated into proteins (Chen 2016; Beermann et al. 2016). Mounting evidence has indicated that lncRNAs play important roles in carcinogenesis and regulate various biological processes, such as cell apoptosis, growth, migration, invasion and metastasis (Kopp and Mendell 2018; Palazzo and Koonin 2020). Furthermore, increasing numbers of lncRNAs have been reported to be associated with early clinical diagnosis and response to therapy in various cancer types (Schmitt and Chang 2016; Dragomir et al. 2020). Many aberrant lncRNA expression signatures have been linked to the carcinogenesis and progression of renal cancer, contributing to new insights into our understanding of genitourinary malignancies (Flippot et al. 2019; Barth, et al. 2019). Although some lncRNAs have been shown to play roles in ccRCC, the majority of lncRNAs remain unexplored in this disease. Therefore, the validation of lncRNAs as clinical biomarkers in ccRCC has yet to be elucidated.

As previously reported, ADAM metallopeptidase with thrombospondin type 1 motif 9 (ADAMTS9) antisense RNA 1 (ADAMTS9-AS1) is located on chromosome 3p14.1. ADAMTS9-AS1 is the antisense transcript of ADAMTS9, and downregulation of ADAMTS9-AS1 has been found in several cancers, such as colon cancer (Li et al. 2020), breast cancer (Fang et al. 2020), and prostate cancer (Wan et al. 2019). Nevertheless, the functional roles and potential mechanism of ADAMTS9-AS1 in ccRCC remain completely unknown. Furthermore, compared with its biological functions, much less is known about the underlying mechanisms of ADAMTS9-AS1 downregulation in cancers. The inhibition of tumor suppressors via epigenetic regulation has been recognized as a major mechanism underlying tumorigenesis and likely occurs at very early stages of oncogenesis in multiple cancers, including RCC (Larkin et al. 2012; Cubas and Rathmell 2018; Maher 2013). This prompted us to investigate whether ADAMTS9-AS1 is suppressed by epigenetic mechanisms, such as promoter hypermethylation, in ccRCC.

ADAMTS9 is one of the ADAMTS protease family members and is a secreted mammalian metalloprotease (Dubail and Apte 2015). ADAMTS9 is a newly discovered tumor suppressor gene (Shao, et al. 2018; Lung et al. 2008) that plays an important role in tumorigenesis and progression in a variety of cancers. For example, ADAMTS9 functions as a tumor suppressor by inhibiting the oncogenic AKT/mTOR signaling pathway (Du et al. 2013; Chen et al. 2017). Furthermore, compared with its biological functions, much less is known about the underlying expression regulatory mechanisms of ADAMTS9 in cancers. However, whether ADAMTS9-AS1 plays any role in ADAMTS9 regulation remains unknown.

In this study, we analyzed the expression of ADAMTS9-AS1 in ccRCC and investigated the mechanisms underlying ADAMTS9-AS1 suppression by examining the methylation

status of the ADAMTS9-AS1 promoter. We also investigated that ADAMTS9-AS1 was inhibits tumor growth and drug resistance. In addition, ADAMTS9-AS1 directly bound to HuR. Then, HuR was guided to the mRNA of ADAMTS9 in an RNA–RNA sequence specific binding manner, resulting in attenuated tumor growth and drug resistance. Therefore, ADAMTS9-AS1 may be a potential marker and therapeutic target for ccRCC patients.

Results

ADAMTS9-AS1 downregulated is associated with poor prognosis in ccRCC

To investigate the expression and clinical significance of ADAMTS9-AS1 in cancer tissues, we first examined its expression levels in human cancer by analyzing the TCGA database. The data demonstrated that ADAMTS9-AS1 was significantly downregulated in pan-cancer samples compared with normal samples (Additional file 1: Figure S1A). The results also indicated that ADAMTS9-AS1 expression was significantly inhibited in most types of cancers, including lung, renal, and colon cancer (Additional file 1: Figure S1B). A negative association between ADAMTS9-AS1 and TNM stages was also observed in many pan-cancer samples (Additional file 1: Figure S1C), including ccRCC (Additional file 1: Figure S1D). Low ADAMTS9-AS1 expression was also associated with significantly poorer outcomes in ccRCC patients (Additional file 1: Figure S1E).

To further study the relationship between ADAMTS9-AS1 expression and cancer prognosis in ccRCC. We measured the expression of ADAMTS9-AS1 in 50 pairs of ccRCC and corresponding adjacent normal tissues (Figure S4). ADAMTS9-AS1 expression was significantly decreased in 72% (36 in total) of the tumors (Fig. 1A). Consistent with the in vivo data described above, ADAMTS9-AS1 was significantly decreased in cancer cell lines in comparison with HK2 normal kidney controls (Fig. 1B). To further understand whether ADAMTS9-AS1 downregulation is involved in ccRCC progression, we examined the expression of ADAMTS9-AS1 in ccRCC tissues of different TNM stages. We found no significant correlation between ADAMTS9-AS1 expression and pathological characteristics, such as age and sex, but did observe that decreased ADAMTS9-AS1 was significantly associated with a higher ccRCC TNM stage, grade and metastasis (Table 1 and Fig. 1C). ccRCC patients with lower ADAMTS9-AS1 expression showed poorer overall survival (Fig. 1D). Furthermore, we also evaluated the prognostic value of ADAMTS9-AS1 using receiver operating characteristic (ROC) curves, which showed that tumor stage, grade, and ADAMTS9-AS1 expression could be regarded as significant prognostic factors with areas under the ROC curve (AUCs) of 0.7122, 0.7255, and 0.7103, respectively (Fig. 1E-F). Combination of ADAMTS9-AS1 expression with TNM stage or grade, with areas under the curve of 0.8166 and 0.7988, respectively, was better as a prognostic factor than stage or grade alone (Fig. 1F). These data together suggest that decreased ADAMTS9-AS1 might contribute to ccRCC pathological progression and could be a potential prognostic factor for ccRCC.

Promoter hypermethylation contributes to ADAMTS9-AS1 silencing in ccRCC

To understand the potential mechanisms that contribute to ADAMTS9-AS1 silencing in ccRCC and pan-cancer tissues, we first examined its DNA methylation levels by analyzing the TCGA database. As expected, we observed significant hypomethylation
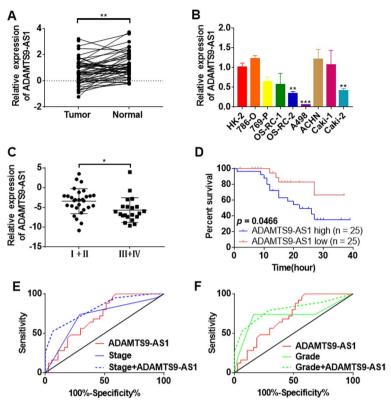
Fig. 1 ADAMTS9-AS1 is downregulated in ccRCC and is associated with poor prognosis. **A**. The expression levels of ADAMTS9-AS1 were detected by qRT-PCR in ccRCC and paired adjacent normal tissues ($n = 50$). **B**. The expression levels of ADAMTS9-AS1 were detected by qRT-PCR in ccRCC cell lines and HK-2 normal kidney cells. **C**. The expression levels of ADAMTS9-AS1 were detected by qRT-PCR in ccRCC of different stages ($n = 50$). **D**. Kaplan–Meier survival analysis of ccRCC patients with low or high expression of ADAMTS9-AS1 (low ADAMTS9-AS1, $n = 25$, high ADAMTS9-AS1, $n = 25$). **E**, **F**. ROC curves showing the AUROC of the combined ADAMTS9-AS1 expression and TNM stage or grade model versus AUROCs of TNM stage, grade or ADAMTS9-AS1 expression alone. The data derived from three independent experiments are presented as mean $\pm$ SEM in the bar graph (**B**). Controls were normalized to 1 (**B**). *$P < 0.05$, **$P < 0.01$

of the ADAMTS9-AS1 promoter in both the pan-cancer (Fig. 2A) and ccRCC tissues (Fig. 2B) compared with normal tissues. The cancer samples were used to calculate the correlation between ADAMTS9-AS1 methylation status and its expression. The results show that ADAMTS9-AS1 promoter methylation is negatively correlated with ADAMTS9-AS1 expression in ccRCC (Fig. 2C).

To further confirm the relationship between ADAMTS9-AS1 and DNA methylation in ccRCC, we treated ccRCC cells with 5-aza-2'-deoxycytidine (5-aza-2′dC), an effective DNA methylation inhibitor, and examined the resultant effects on ADAMTS9-AS1 transcripts. In A498 cells, which express relatively low levels of ADAMTS9-AS1, 5-aza-2′dC treatment restored the transcription of ADAMTS9-AS1 in a concentration-dependent manner (Fig. 2D). However, 786-O cells, which express relatively high levels of ADAMTS9-AS1, were unaffected by the treatment (Fig. 2E). These data indicate that promoter hypermethylation may be one of the major mechanisms by which ADAMTS9-AS1 transcription is inhibited, particularly in ccRCC cells with relatively low levels of ADAMTS9-AS1.

Zhao *et al. Cancer Nanotechnology*   (2023) 14:57

Page 5 of 24

Table 1 Associations of ADAMTS9-AS1 expression with clinicopathological factors

Characteristics	Number of patients	ADAMTS9-AS1		χ2	*P* value
		High expression (%)	Low expression (%)		
Gender				3	0.083
Male	20	7(28.00)	13(52.00)		
Female	30	18(72.00)	12(48.00)		
Age				2.381	0.123
≤65	35	20(80.00)	15(60.00)		
>65	15	5(20.00)	10(40.00)		
TNM stage				10.272	0.001
I+II	31	10(40.00)	21(84.00)		
III+IV	19	15(60.00)	4(16.00)		
Grade				6.876	0.009
Grade 1+2	31	11(44.00)	20(80.00)		
Grade 3+4	19	14(56.00)	5(20.00)		
Lymph node metastasis				7.714	0.005
No	35	13(52.00)	22(88.00)		
Yes	15	12(48.00)	3(12.00)		
Distant metastasis				6.818	0.009
M0	44	19(76.00)	25(100.00)		
M1	6	6(24.00)	0(0.00)		

P value when expression levels were compared using the Pearson Chi-square test

ADAMTS9-AS1 inhibits ccRCC cell viability in vitro

We next investigated the roles of ADAMTS9-AS1 in regulating cell growth in ccRCC. First, ADAMTS9-AS1 was stably overexpressed by lentiviral infection in A498 and OS-RC-2 cells (Fig. 3A and Additional file 1: Figure S2A), which express relatively low levels of endogenous ADAMTS9-AS1. Then, cell growth was measured by CCK-8 and colony formation assays. ADAMTS9-AS1 overexpression significantly inhibited cell viability, suggesting that ADAMTS9-AS1 regulates cell growth (Fig. 3B and Additional file 1: Figure S2B). Then, we used two independent small interfering shRNAs to knock down ADAMTS9-AS1 in A498 and OS-RC-2 cells. As shown in Fig. 3A and Additional file 1: Figure S2A, both ADAMTS9-AS1-specific shRNA significantly reduced ADAMTS9-AS1 expression in A498 and OS-RC-2 cells. Then, cell growth was measured by CCK-8 and colony formation assays. ADAMTS9-AS1 inhibition significantly enhanced cell growth rates in both cell lines (Fig. 3C and Additional file 1: Figure S2C). These data together suggest that ADAMTS9-AS1 inhibits ccRCC growth in vitro.

ADAMTS9-AS1 affects ccRCC sensitivity to 5-aza-dC in vitro

ADAMTS9-AS1 was downregulated in ccRCC mainly due to promoter hypermethylation. 5-Aza-dC, a DNA demethylation agent that is frequently utilized in human clinical trials (Agrawal et al. 2018), could restore the expression of ADAMTS9-AS1 in ccRCC cells. Drug resistance is one of the major obstacles to treating ccRCC (Mijn et al. 2014), therefore we explored the influence of ADAMTS9-AS1 on the response of ccRCC cells to 5-aza-dC-induced cell death. We found that the viability of A498 and
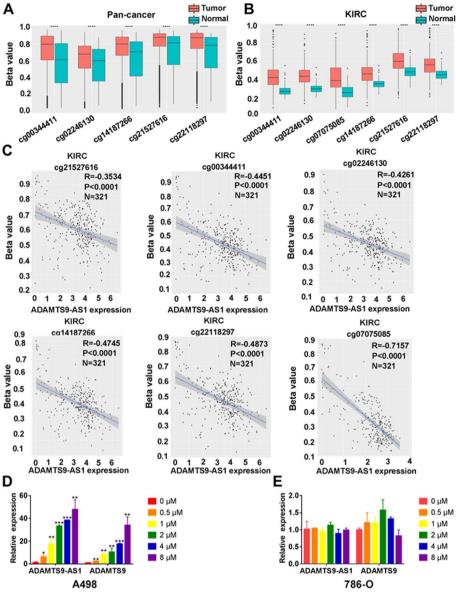
Fig. 2 Promoter hypermethylation contributes to ADAMTS9-AS1 silencing in ccRCC. **A**-**B**. The DNA methylation values of ADAMTS9-AS1 were performed in pan-cancer and kidney renal clear cell carcinoma (KIRC) samples from the TCGA database. **C**. The RNA expression and DNA methylation levels of ADAMTS9-AS1 showed a negative linear correlation in KIRC samples from the TCGA database. **D**-**E**. The expression levels of ADAMTS9-AS1 in A498 (**D**) and 786-O (**E**) cell lines were obtained by qRT-PCR after treatment with different doses of 5-aza-dC. The data derived from three independent experiments are presented as mean ± SEM in the bar graphs (**D**-**E**). Controls were normalized to 1 (D-E). *$P < 0.05$, **$P < 0.01$, ***$P < 0.001$, N.S. not significant

OS-RC-2 cells was reduced by 5-aza-dC in a dose-dependent manner in ADAMTS9-AS1 stable lines compared with the corresponding vector controls (Fig. 3D and Additional file 1: Figure S2D). In contrast, cell viability was enhanced after ADAMTS9-AS1 KD in A498 and OS-RC-2 cells (Fig. 3D and Additional file 1: Figure S2D), suggesting that ADAMTS9-AS1 enhances ccRCC sensitivity to 5-aza-dC. Furthermore, ADAMTS9-AS1 significantly enhanced apoptosis rates, as shown by Annexin V/PI
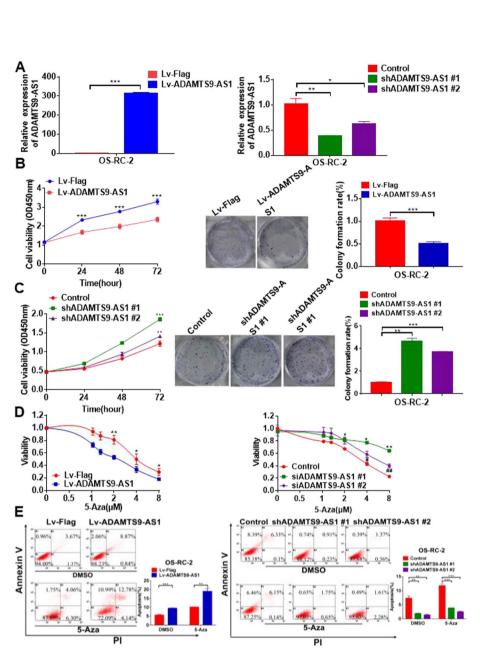
Fig. 3 ADAMTS9-AS1 inhibits ccRCC cell viability and sensitivity to 5-aza-dC in vitro. **A**. ADAMTS9-AS1 overexpression and KD efficiency was confirmed by qRT-PCR in A498 cells. **B**-**C**. Cell growth was determined by CCK-8 (left) and colony formation (right) assays following ADAMTS9-AS1 overexpression (**B**) and KD (**C**) in A498 cells. **D** Cell viability of A498 cells were detected by CCK-8 assay following ADAMTS9-AS1 overexpression (left) or ADAMTS9-AS1 knockdown (right) and treatment with a concentration gradient of 5-aza- dC. **E** The apoptosis ratio was detected by FACS assay following ADAMTS9-AS1 overexpression (left) or ADAMTS9-AS1 knockdown (right) in A498 cells with or without 5-aza-dC treatment. The data derived from three independent experiments are presented as mean ± SEM in the bar graphs **A**–**E**. Controls were normalized to 1 (**A**–**D**). *$P < 0.05$, **$P < 0.01$, ***$P < 0.001$

double staining following 5-aza-dC treatment (Fig. 3E and Additional file 1: Figure S2E). Importantly, these effects were compromised by ADAMTS9-AS1 KD (Fig. 3E and Additional file 1: Figure S2E). These data suggest that ADAMTS9-AS1 is required to enhance the efficacy of 5-aza-dC in ccRCC.

ADAMTS9-AS1 inhibits tumor growth and resistance to 5-aza-dC in vivo

To investigate the effect of ADAMTS9-AS1 on cancer growth in vivo, we utilized xenograft mouse models. We first infected A498 cells with the scramble control (Lv-Flag) or ADAMTS9-AS1 (Lv-ADAMTS9-AS1) lentivirus and confirmed ADAMTS9-AS1 upregulation by qRT-PCR (Fig. 3A). Control and ADAMTS9-AS1-overexpressing cells were injected into nude mice at symmetrical subcutaneous regions. Two weeks after tumor cell injection, ADAMTS9-AS1 overexpressing tumors were significantly smaller than controls (Fig. 4A-B, Additional file 1: Figure S5A); this effect became more pronounced over time. At the end of the experiment, the mice were dissected, and tumor weights were immediately measured. Overexpression of ADAMTS9-AS1 significantly inhibited the tumor weight compared with the control group (Fig. 4C). In contrast, ADAMTS9-AS1 KD in A498 cells significantly enhanced the tumor volume and tumor weight of xenografts (Fig. 4D-F, Additional file 1: Figure S5B). These data together suggest that ADAMTS9-AS1 inhibits ccRCC growth in vivo.

To investigate the effect of ADAMTS9-AS1 on cancer drug resistance in vivo, we administered 2.0 mg/kg of 5-aza-dC. Tumor volumes and weights were reduced in the 5-aza-dC treatment group compared with those in the control group. Upon treatment with 5-aza-dC, ADAMTS9-AS1 KD xenografts displayed significantly increased tumor volumes and weights compared with control xenografts (Fig. 4D–F). 5-Aza-dC treatment had no influence on body weight (Fig. 4G), indicating that ADAMTS9-AS1 enhances ccRCC sensitivity to 5-aza-dC in vivo. In agreement with the in vitro data, ADAMTS9-AS1 expression was elevated by 5-aza-dC in vivo (Fig. 4H). These data further support a model in which ADAMTS9-AS1 is required to enhance the efficacy of 5-aza-dC in ccRCC.

ADAMTS9-AS1 affects ADAMTS9 mRNA stability in ccRCC

Most lncRNAs can perform their functions by regulating nearby genes (Yao et al. 2019). ADAMTS9-AS1 is an antisense RNA of ADAMTS9. To further investigate the underlying mechanisms by which ADAMTS9-AS1 regulates cell growth and drug resistance, we explored the relationship between ADAMTS9-AS1 and ADAMTS9. We found that overexpression of ADAMTS9-AS1 elevated ADAMTS9 mRNA and protein levels (Fig. 5A-B), while ADAMTS9-AS1 KD inhibited ADAMTS9 expression (Fig. 5C-D). It is also worth noting that ADAMTS9-AS1-mediated ADAMTS9 activation has similar effects to those observed with or without 5-aza-dC treatment in ccRCC xenograft models (Fig. 5E–H). In addition, ADAMTS9-AS1 induced ADAMTS9 expression is not at transcription levels, due to neither ectopic ADAMTS9-AS1 expression or KD had a significant effect on the luciferase activity of ADAMTS9 promoter (Fig. 5I). More importantly, the half-life of ADAMTS9 was increased through ADAMTS9-AS1 overexpression (Fig. 5J). Collectively, these findings indicate that ADAMTS9-AS1 enhances the ADAMTS9 mRNA stability.

ADAMTS9-AS1 is physically associated with HuR

To explore the potential mechanisms of ADAMTS9-AS1 regulating the ADAMTS9 mRNA stability, we performed a biotin-labeled RNA pull-down assay followed by silver
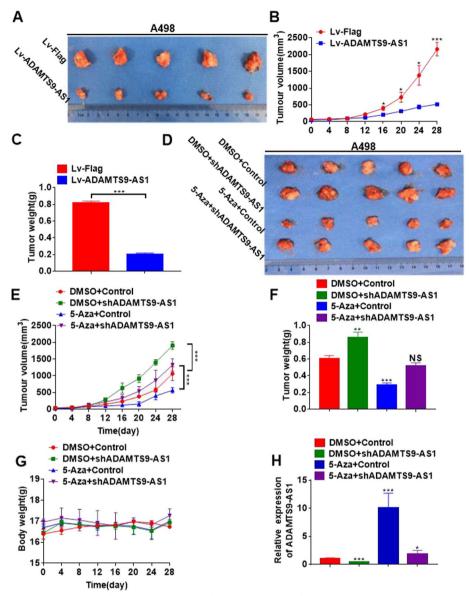
Zhao *et al. Cancer Nanotechnology*   (2023) 14:57

Page 9 of 24

Fig. 4 ADAMTS9-AS1 inhibits tumor growth and resistance to 5-aza-dC in vivo. **A**–**C**. Tumor images (A), volumes (B), and tumor weights at the experimental endpoint (**C**) were compared between Lv-Flag and ADAMTS9-AS1 in A498 xenograft. Error bars, mean ± SD ($n = 5$ for each group). **D**–**G** Tumor images (**D**), volumes (**E**), tumor weights at the experimental endpoint (**F**), and body weights (**G**) were compared between control and shADAMTS9-AS1 in A498 xenograft with DMSO or 5-aza-dC treatment. ($n = 5$ for each group). **H** The expression levels of ADAMTS9-AS1 were detected by qRT-PCR in in A498 xenograft tissues with DMSO or 5-aza-dC treatment. The data derived from three independent experiments are presented as the mean ± SEM in the bar graph (**H**). Controls were normalized to 1 (**H**). *$P < 0.05$, **$P < 0.01$. ***$P < 0.001$, N.S. not significant

staining (Fig. 6A). An approximately 40-kDa band was analysis via mass spectrometry in ADAMTS9-AS1 group. HuR, an RNA binding protein that generally regulates RNA stability, as a ADAMTS9-AS1 binding protein in the analyzing data (Additional file 1: Figure S3A). HuR was a specific binding protein for biotin-labeled ADAMTS9-AS1 conformed by WB (Fig. 6B). Bioinformatic analysis also provides evidence for the binding of HuR and ADAMTS9-AS1 through the catRAPID website (Additional file 1: Figure
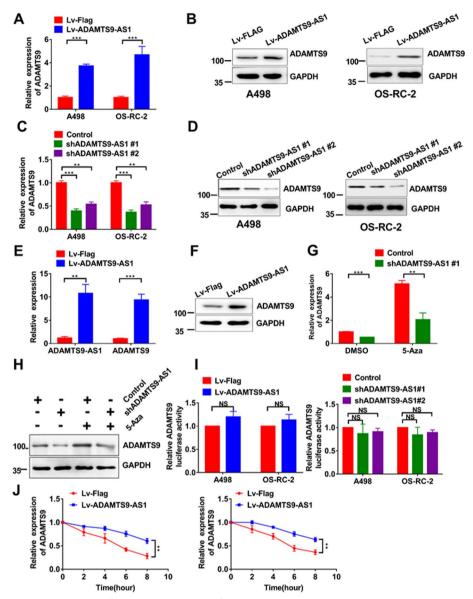
Fig. 5 ADAMTS9-AS1 affects the mRNA stability of ADAMTS9 in ccRCC. **A**, **C**. The mRNA expression levels of ADAMTS9 were detected by qRT-PCR in A498 and OS-RC-2 cells following ADAMTS9-AS1 overexpression (**A**) and KD (**C**). **B**, **D**. The protein expression levels of ADAMTS9 were detected by WB in A498 and OS-RC-2 cells following ADAMTS9-AS1 overexpression (**B**) and KD (**D**). (**E**). The expression levels of ADAMTS9 and ADAMTS9-AS1 were detected by qRT-PCR in an ADAMTS9-AS1 overexpression xenograft model. (**F**). The protein expression levels of ADAMTS9 were detected by WB in the ADAMTS9-AS1 overexpression xenograft model. **G**-**H**. The mRNA (**G**) and protein (H) expression levels of ADAMTS9 were detected by qRT-PCR in ADAMTS9-AS1 knockdown xenografts with or without 5-aza-dC treatment. **I**. ADAMTS9 promoter luciferase reporter activity was detected by luciferase reporter assay after ADAMTS9-AS1 overexpression or KD. **J**. The half-life of ADAMTS9 mRNA was measured by qRT-PCR in the presence of ActD treatment in A498 (left) and OS- RC-2 (right) cells. The data derived from three independent experiments are presented as the mean ± SEM in the bar graphs (**A**, **C**, **E**, **G**, **I**, **J**). Controls were normalized to 1 (**A**, **C**, **E**, **G**, **I**, **J**). **$P < 0.01$, ***$P < 0.001$. N.S. not significant

S3B). To investigate the interaction under physiological conditions, the binding between ADAMTS9-AS1 and HuR was further measured by UV cross-linking and immunoprecipitation (CLIP). The results show that ADAMTS9-AS1, but not GAPDH RNA, was
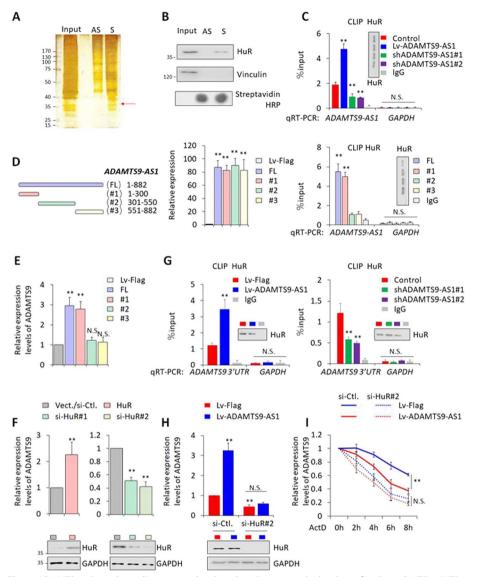
Fig. 6 ADAMTS9-AS1 is physically associated with HuR and increases the binding of HuR to ADMTS9 3'UTR. **A**. RNA pull-down assay by ADAMTS9-AS1 and its antisense RNA followed by silver staining of protein extract from A498 cells. A band indicated by an arrow was excised for mass spectrometry analysis. S: sense strand of ADAMTS9-AS1, AS: antisense strand of ADAMTS9-AS1. **B**. Western blot analysis of the specific association of HuR and ADAMTS9-AS1. Vinculin was used as the negative control. The same amount of sense and antisense ADAMTS9-AS1 transcripts confirmed by dot-blot assay. **C**. ADAMTS9-AS1 associated HuR was measured by qRT-PCR following CLIP HuR after ADAMTS9-AS1 overexpression or KD in A498 cells. *GAPDH* and CLIP IgG were used as negative controls. HuR pull-down efficiency was determined by WB. **D**. Schematic diagram of the full-length and truncated ADAMTS9-AS1(left). CLIP assay was used to detect the binding of HuR with full-length or fragmented ADAMTS9-AS1 after overexpression of the indicated ADAMTS9-AS1. CLIP IgG and *GAPDH* were used as negative controls (right). Similar expression levels of ADAMTS9-AS1 were confirmed by qRT-PCR (middle). HuR pull-down efficiency was determined by WB. **E**, **F**. The mRNA expression levels of ADAMTS9 were determined by qRT-PCR after truncated ADAMTS9-AS1 (**E**) and HuR (**F**) overexpressed or HuR KD (**F**) in in A498 cells. The transfection efficiency of HuR was measured by WB(F). (**G**). ADAMTS9 associated HuR was measured by qRT-PCR following CLIP HuR after ADAMTS9-AS1 overexpression or KD in A498 cells. *GAPDH* and CLIP IgG were used as negative controls. HuR pull-down efficiency was determined by WB. **H**-**I**. The expression levels (**H**) and the half-life (**I**) of ADAMTS9 mRNA of ADAMTS9 were determined by qRT-PCR after HuR KD in Control and ADAMTS9-AS1 overexpressed cells. The data derived from three independent experiments are presented as the mean ± SEM in the bar graphs (**C**–**I**). Controls were normalized to 1 (**D**, **E**, **F**, **H**, **I**). $**P < 0.01$, $***P < 0.001$. N.S. not significant

physically binding with HuR. Furthermore, the association of HuR with ADAMTS9-AS1 was enhanced by ADAMTS9-AS1 overexpression and decreased with ADAMTS9-AS1 KD (Fig. 6C), suggesting the specific interaction between HuR and ADAMTS9-AS1. We further mapped the sequence in ADAMTS9-AS1 that potentially contributes to their interaction. The similar expression of ADAMTS9-AS1 or ADAMTS9-AS1 fragments were overexpressed (Fig. 6D). Full-length and (1–300 nt) ADAMTS9-AS1#1 were associated with HuR (Fig. 6D). Importantly, mRNA expression levels of ADAMTS9 were induced by full-length and (1–300 nt) ADAMTS9-AS1 (Fig. 6E). To investigate possible effects of ADAMTS9-AS1 on HuR expression, the results showed that ADAMTS9-AS1 did not have ability to change HuR expression by ADAMTS9-AS1 overexpressing or KD (Additional file 1: Figure S3C). Therefore, ADAMTS9-AS1 was physically associated with HuR by 1–300 nt.

ADAMTS9-AS1 increases the binding of HuR to ADMTS9 3'UTR

Next, we will verify whether HuR can regulate the expression of ADAMTS9. We found that overexpression of HuR elevated ADAMTS9 mRNA and protein levels (Fig. 6F), while HuR KD inhibited ADAMTS9 expression (Fig. 6F). A CLIP assay and bioinformatic analysis revealed that HuR was associated with ADMTS9 3'UTR (Fig. 6G and Additional file 1: Figure S3D). These data indicate that HuR is recruited to ADMTS9 3'UTR to enhance its expression.

We wondered whether ADAMTS9-AS1 contributes to the recruitment of HuR to the ADMTS9 3'UTR. We measured the binding of HuR to ADMTS9 3'UTR in ADAMTS9-AS1 overexpression and KD cells. The results showed that the association of HuR with ADAMTS9 was enhanced by ADAMTS9-AS1 overexpression and decreased with ADAMTS9-AS1 KD (Fig. 6G). In addition, in order to verify whether ADAMTS9-AS1 regulates the expression of ADAMTS9 dependent on HuR, we found that the regulatory effect of ADAMTS9-AS1 on ADAMTS9 disappeared in HuR KD cells (Fig. 6H). Consistently, the HuR KD inhibited ADAMTS9's half-life and abolished ADAMTS9-AS1 induced effects (Fig. 6I). Collectively, these data suggest that ADAMTS9-AS1 facilitates HuR recruitment in the ADMTS9 3'UTR.

ADAMTS9-AS1 guides HuR by forming an RNA–RNA complex with ADAMTS9 3'UTR

To further explore the molecular mechanisms of ADAMTS9-AS1 guiding HuR to the ADMTS9 3'UTR. One possible reason is that ADAMTS9-AS1 physically associate with ADMTS9 3'UTR via formation an RNA–RNA complex. To test this, three major binding sites of ADAMTS9-AS1 and ADAMTS9 3'UTR were predicted by using bioinformatic websites, IntaRNA (Fig. 7A). The association between ADAMTS9-AS1 and ADMTS9 3'UTR was performed by RNA–RNA interaction assay, the results show that ADMTS9 3'UTR was indeed binding the ADAMTS9-AS1, and the major binding regions is ADAMTS9-AS1#3 (551–882 nt), a region containing the NO3 binding site, whereas no obvious association with NO1(ADAMTS9-AS1#1) and NO2(ADAMTS9-AS1#2) binding sites (Fig. 7B).

To better understand which predicted binding sites of ADMTS9 3'UTR contribute to the interaction with ADAMTS9-AS1, full-length ADMTS9 3'UTR and three truncated ADMTS9 3'UTR mutants were labeled with biotin in vitro. ADAMTS9-AS1 bound with
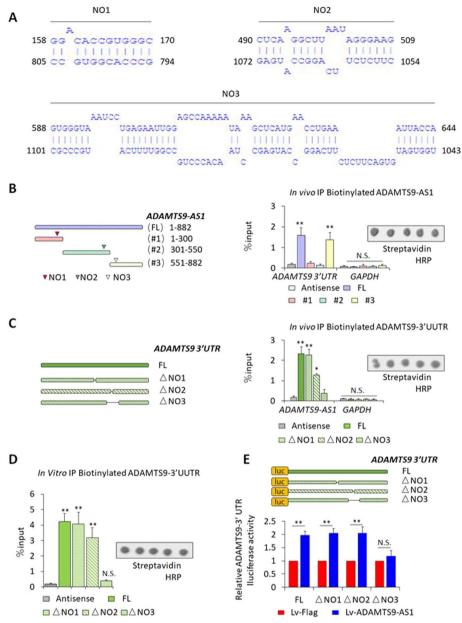
Fig. 7 ADAMTS9-AS1 guides HuR by forming an RNA–RNA complex with ADAMTS9 3′UTR. **A**. The binding sites of ADAMTS9-AS1 and ADAMTS9 3′UTR were predicted by website (IntaRNA). **B**. Schematic of the predicted positions of ADAMTS9 3′UTR binding sites in ADAMTS9-AS1 (left). RNA–RNA interaction assay was used to detect the binding of biotin-labeled full-length or truncated ADAMTS9-AS1 and ADAMTS9 3′UTR in A498 cells (right). The same amount of biotin-full-length or truncated ADAMTS9-AS1 transcripts confirmed by dot-blot assay. **C**. Schematic of the predicted positions of ADAMTS9-AS1 binding sites in ADAMTS9 3′UTR (left). RNA–RNA interaction assay was used to detect the binding of biotin-labeled full- length or truncated ADAMTS9 3′UTR and ADAMTS9-AS1 in A498 cells(right). The same amount of biotin-full-length or truncated ADAMTS9 3′UTR transcripts confirmed by dot-blot assay. **D**. RNA–RNA interaction assay was used to determine the biotin-labeled ADAMTS9-AS1#3 (551–882 nt) directly binding with full-length or truncated ADAMTS9 3′UTR in vitro. The same amount of biotin-full-ADAMTS9-AS1#3 transcripts confirmed by dot-blot assay. **E**. Full-length and truncated ADAMTS9 3′UTR luciferase activities were measured by luciferase reporter assay in ADAMTS9-AS1 overexpressed A498 cells. The data derived from three independent experiments are presented as the mean ± SEM in the bar graphs (**B**–**E**). Controls were normalized to 1 (**E**). *$P < 0.05$, **$P < 0.01$, N.S. not significant

all ADMTS9 3'UTR mutants except ADMTS9 3'UTR△NO3, suggesting that ADMTS9 3′UTR binds with ADAMTS9-AS1 through NO3 domain (Fig. 7C). This was not due to differing ADMTS9 3′UTR pull-down efficiency, because a similar amount of biotinylated ADMTS9 3'UTR was precipitated. Therefore, we assumed that ADAMTS9-AS1#3 was associated with NO3 (1043–1101 nt) sequence of ADMTS9 3'UTR. To this end, biotinylated ADAMTS9-AS1#3 mixed with truncated ADMTS9 3'UTR mutants. We found that ADAMTS9-AS1 was associated with all ADMTS9 3'UTR mutants except ADMTS9 3'UTR△NO3, suggesting that ADAMTS9-AS1 directly binds with NO3 domain of ADAMTS9 3′UTR (Fig. 7D). In addition, ADAMTS9-AS1 promotes all ADMTS9 3′UTR mutants luciferase activity except ADMTS9 3′UTR△NO3 mutants (Fig. 7E).

These data indicated that ADAMTS9-AS1 forms a RNA–RNA complex with ADMTS9 3'UTR through NO3 binding sites.

The ADAMTS9-AS1/ADAMTS9 axis inhibits ccRCC cell growth and drug resistance

To identify the association between ADAMTS9-AS1 and ADAMTS9 mRNA levels in cancer pathogenesis, we found that the mRNA expression of ADAMTS9 was 7.32-fold downregulated in ccRCC compared with their paired adjacent normal controls (Fig. 8A). Consistent with the in vivo data described above, ADAMTS9 was significantly decreased in cancer cell lines in comparison with HK2 normal kidney controls (Fig. 8B). Interestingly, ccRCC samples with lower ADAMTS9 mRNA transcript levels tended to express lower amounts of ADAMTS9-AS1 (Fig. 8C). However, consistent with the results by analyzing TCGA database, reduced ADAMTS9-AS1 levels were significantly correlated with decreased ADAMTS9 mRNA expression in ccRCC (Fig. 8D). These data suggest that the inhibition of ADAMTS9 may be at least in part dependent on ADAMTS9-AS1 downregulation in ccRCC.

Based on the positive relationship between ADAMTS9-AS1 and ADAMTS9 in human ccRCC specimens, we conducted in vitro experiments to investigate whether ADAMTS9 functions in an ADAMTS9-mediated manner in ccRCC. The CCK-8 assay results showed that overexpression of ADAMTS9-AS1 inhibited cell growth (Fig. 8E). Interestingly, ADAMTS9 KD partially abolished the effect of ADAMTS9-AS1 overexpression (Fig. 8E). The CCK-8 and apoptosis assays also showed that ADAMTS9 knockdown partially attenuated the effects of ADAMTS9-AS1 overexpression on the sensitivity of ccRCC to 5-aza-dC (Fig. 8F-G). These data indicate that ADAMTS9-AS1 attenuates cell proliferation and drug resistance in an ADAMTS9-mediated manner.

Discussion

RCC is known for its high resistance to chemotherapeutic drugs, resulting in a lack of effective treatments for advanced disease (George et al. 2019). There is an urgent need for new therapeutic targets to overcome drug resistance (Nikolaou et al. 2018). The discovery of important functions of protein-coding genes has led to great success in the development of targeted therapies for cancer (McLysaght and Hurst 2016). Accumulating evidence indicates that abnormal lncRNAs play multiple roles in maintaining tumor initiation and progression, demonstrating their clinical potential as biomarkers and therapeutic targets (Huarte 2015). These discoveries have stimulated
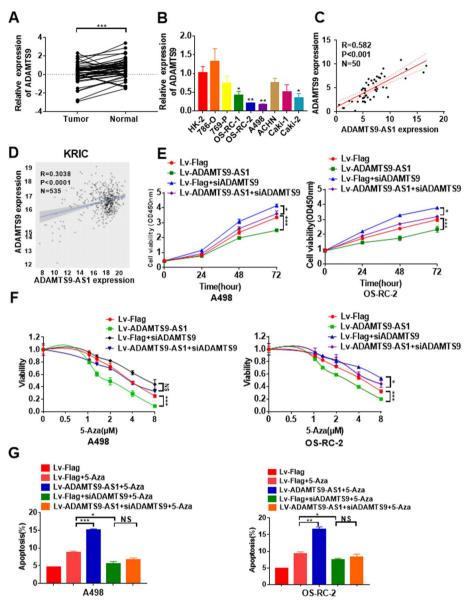
Fig. 8 The ADAMTS9-AS1/ADAMTS9 axis inhibits ccRCC cell growth and drug resistance. **A**-**B**. The mRNA expression levels of ADAMTS9 were detected by qRT-PCR in ccRCC tissues ($n = 50$) (**A**) and ccRCC cell lines (B). **C**-**D**. ADAMTS9 mRNA and ADAMTS9-AS1 expression levels showed a positive linear correlation in ccRCC tissues (**C**) and TCGA database (**D**). **E**-**F**. A498 and OS-RC-2 cell viability was detected by CCK-8 assay after ADAMTS9-AS1 overexpression or ADAMTS9 knockdown with (**F**) or without (**E**) 5-aza- dC treatment. **G** A498 and OS-RC-2 apoptosis rates were detected by FACS following ADAMTS9-AS1 overexpression or ADAMTS9 knockdown with or without 5-aza-dC. The data derived from three independent experiments are presented as the mean ± SEM in the bar graphs (**B**, **E**, **F**, **G**). Controls were normalized to 1 (B, E, F, G). *$P < 0.05$, **$P < 0.01$, ***$P < 0.001$

great interest in investigating the function and regulation of lncRNAs to improve the diagnosis and treatment of cancer (Lin and Yang 2018; Slack and Chinnaiyan 2019). In recent years, emerging evidence has revealed that the lncRNA ADAMTS9-AS1, the antisense transcript of ADAMTS9, is a tumor suppressor gene. Downregulation of ADAMTS9-AS1 participates in the development of various tumors (Fang et al.

Zhao *et al. Cancer Nanotechnology*   (2023) 14:57

Page 16 of 24

2020; Chen et al. 2020). However, it remains unclear whether ADAMTS9-AS1 plays a tumor suppressive role in ccRCC.

In this study, bioinformatics analyses indicated that ADAMTS9-AS1 was significantly downregulated and had a negative association with TNM stage across cancers. In addition, decreased ADAMTS9-AS1 was also associated with significantly poorer outcomes in many cancer types. Consistent with bioinformatics data, we found that ADAMTS9-AS1 expression is commonly decreased in ccRCC cell lines and tissues. Decreased HITT is associated with advanced stages and poor prognosis in ccRCC patients. Our findings suggest that ADAMTS9-AS1 plays an important role in ccRCC tumorigenesis. In addition, ADAMTS9-AS1 downregulation contributes to 5-aza-dC resistance in ccRCC.

Cell growth and drug resistance are major clinical problems for ccRCC treatment (Shuch et al. 2015). We investigated the potential role and possible regulatory mechanism of ADAMTS9-AS1 in ccRCC. Our data indicated that overexpression of ADAMTS9-AS1 significantly inhibited tumor cell growth in vitro and in vivo. In addition, ADAMTS9-AS1 significantly enhanced apoptosis rates after 5-aza-dC treatment, and these effects were compromised by ADAMTS9-AS1 KD. Our study indicated that ADAMTS9-AS1 may serve as an effective molecular target to block ccRCC development and drug resistance.

We are very curious about the regulatory mechanism of ADAMTS9-AS1 in ccRCC, due to the important function of ADAMTS9-AS1. It is common for lncRNA to regulate the expression of nearby genes (Yan et al. 2017), and ADAMTS9 is the neighboring gene of ADAMTS9-AS1. ADAMTS9 is downregulated in various types of human cancer. ADAMTS9 was reported to be a novel tumor suppressor gene based on its remarkable ability to induce apoptosis and inhibit cell proliferation in nasopharyngeal (Lung et al. 2008), pancreatic (Zhang et al. 2010), gastric (Du et al. 2013), colorectal (Chen et al. 2017) and esophageal squamous cell carcinomas (Lo, et al. 2007). Notably, promoter hypermethylation contributed to the significant downregulation of ADAMTS9 expression in many cancer types (Lung et al. 2008; Peng et al. 2013). However, the other expression regulatory mechanism of ADAMTS9 remains unknown. Considering that ADAMTS9 plays an important role in cancer, whether ADAMTS9-AS1 regulates ADAMTS9 should be further explored. In this study, we found that ADAMTS9-AS1 promoted the stability of ADAMTS9 mRNA. Consistent with this finding, the mRNA expression of ADAMTS9 was dramatically decreased in ccRCC tissues and was positively correlated with ADAMTS9-AS1 expression. Notably, ADAMTS9 partially rescued ADAMTS9-AS1-induced cell growth and drug resistance in ccRCC. To the best of our knowledge, ADAMTS9-AS1 is a newly identified lncRNA involved in the regulation of ADAMTS9. Taken together, these findings suggest that ADAMTS9-AS1/ADAMTS9-regulated cell growth and drug resistance play important roles in ccRCC.

It will be interesting to explore the molecular mechanism by which ADAMTS9-AS1 regulates the mRNA stability of ADAMTS9. LncRNA can be used as a molecular decoy for RNA binding proteins, which are themselves regulators of gene expression (Wang and Chang 2011). HuR is a well-characterized mRNA stability regulator and can either promote or inhibit the stability of its RNA target (Wang et al. 2019a; Yoon et al. 2012).

Some recent articles reported that lncRNA regulates downstream gene expression by binding to HuR (Hao et al. 2019; Wang et al. 2019b). Our data showed that ADAMTS9-AS1 was directly associated with HuR and promote the interaction of HuR with ADAMTS9 3'UTR via forming RNA–RNA complex to enhance ADAMTS9 expression. We found that ADAMTS9-AS1#1(1-300 nt) and ADAMTS9-AS1#3 (551-882 nt) was associated with HuR and ADMTS9 3'UTR NO3 (1043-1101nt), respectively. The potential of RNA to bind RNA sequences suggests that lncRNAs play an important 'guiding' role. As such, the ADAMTS9-AS1-ADMTS9 3'UTR guides HuR specifically to its target site, resulting in ADMTS9 mRNA stability activation.

Considering that ADAMTS9-AS1 plays an important role in inhibiting cell growth and drug resistance in ccRCC, we sought to discover strategies to restore ADAMTS9-AS1 expression by exploring potential mechanisms of ADAMTS9-AS1 suppression in ccRCC. In this study, analysis of the TCGA database indicated that the ADAMTS9-AS1 promoter is hypermethylated in pan-cancer tissues compared to normal tissues. Reduced ADAMTS9-AS1 expression is closely associated with promoter methylation across cancers. Consistent with this finding, our data suggest that ADAMTS9-AS1 transcription could be restored by demethylation treatment in ccRCC cells with relatively low endogenous ADAMTS9-AS1 expression. These data indicate that promoter hypermethylation may be one of the major mechanisms by which ADAMTS9-AS1 transcription is inhibited, particularly in ccRCC. Whether ADAMTS9-AS1 expression can be induced by demethylation treatment in other tumors requires further investigation.
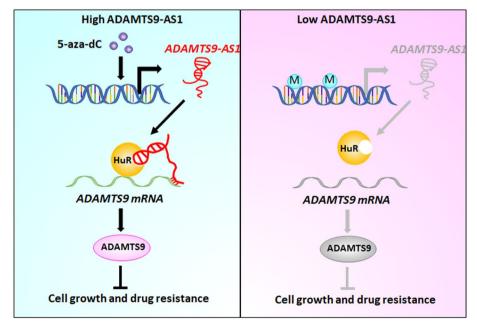

Fig. 9 Schematic diagram of ADAMTS9-AS1 regulation and function in ccRCC, ADAMTS9-AS1-HuR–ADAMTS9 axis inhibits cell growth and drug resistance. The suppression of ADAMTS9-AS1 in ccRCC is mainly due to promoter hypermethylation. 5-Aza-2'dC, an effective DNA methylation inhibitor, efficiently restores ADAMTS9-AS1 expression in ccRCC. Higher levels of ADAMTS9-AS1 inhibits tumor growth and drug resistance via recruiting HuR to enhance ADAMTS9 mRNA stability. Lower levels of ADAMTS9-AS1 cannot stabilize ADAMTS9 mRNA, resulting in cell growth and drug resistance

In summary, we identified ADAMTS9-AS1 as a tumor suppressor that is decreased in ccRCC and is associated with advanced stages and poor prognosis in ccRCC patients. Promoter hypermethylation contributes to ADAMTS9-AS1 silencing in ccRCC. ADAMTS9-AS1 suppresses cancer growth and drug resistance through guiding HuR to ADMTS9 3'UTR and stabilized its mRNA (Fig. 9). These findings provide important insights into novel treatment strategies that warrant further investigation in the clinic, particularly for ccRCC patients with ADAMTS9-AS1 downregulation.

Materials and methods

Clinical specimens

ccRCC tissues and their corresponding adjacent normal tissues were obtained from the Second Affiliated Hospital of Harbin Medical University, China. Tissues were snap-frozen in liquid nitrogen and stored at -80 ℃. Each participant provided written informed consent. The use of human clinical tissues was approved by the Research Ethics Committee of Harbin Medical University, China.

Access to and investigation of online cancer datasets

Genome-wide ADAMTS9-AS1 and other gene expression profiles and clinicopathological factors were downloaded from TCGA (https://tcga-data.nci.nih.gov/). Expression of ADAMTS9-AS1 was dichotomized using the median expression as the cutoff, with "high expression" defined as values at or above the median and "low expression" defined as values below the median. Overall survival (OS) was defined as the time from treatment until death or relapse. The log-rank test was used to examine survival differences between patient groups.

Pairwise Pearson correlation was performed to assess correlations between the expression of ADAMTS9-AS1 and all other genes. Only positively correlated genes with an $R \geq 0.4$ and a significant correlation ($P < 0.05$) were retained. Kyoto Encyclopedia of Genes and Genomes (KEGG) pathway analysis was performed using DAVID Functional Annotation Bioinformatics Microarray Analysis (https://david.ncifcrf.gov/).

The DNA methylation profile was measured experimentally using the Illumina Infinium HumanMethylation450 platform and was downloaded from TCGA. Beta values were derived at Johns Hopkins University and the University of Southern California TCGA genome characterization center. DNA methylation values, described as beta values, were recorded for each array probe in each sample via BeadStudio software. DNA methylation beta values are continuous variables between 0 and 1, representing the ratio of the intensity of the methylated bead type to the combined locus intensity. Thus, higher beta values represent higher levels of DNA methylation, and lower beta values represent lower levels of DNA methylation.

All statistical tests were two-tailed, and $P < 0.05$ indicated statistical significance. Statistical analysis was performed using R.3.5.3 software.

Cell culture

All cells were purchased from the Shanghai Cell Bank of the Chinese Academy of Science. 786-O, 769-P, OS-RC-1, OS-RC-2, A498, ACNH, Caki-1 and Caki-2 cells were

maintained in RPMI-1640 medium (Gibco) supplemented with 10% (v/v) fetal bovine serum (Gibco). ACNH cells were grown in Dulbecco's modified Eagle's medium (DMEM) with the same supplements listed above. All cells were grown at 37 °C in a humidified incubator (Thermo Scientific) with 5% CO2. Cell lines were routinely tested for mycoplasma contamination.

Plasmid and lentivirus production and infection

A498 and OS-RC-2 cells were plated at 5×10^6 cells per well in 6-well plates and transfected with ADAMTS9-AS1 lentivirus at an MOI $=10$ in Opti-MEM supplemented with polybrene. Stable cell lines were selected for 5 days with 2.5 µg/mL puromycin. ShRNA or siRNA were transfected into the A498 and OS-RC-2 cell lines using Lipofectamine 2000 (Invitrogen) according to the manufacturer's instructions. All plasmids used were extracted using the Endo-Free Plasmid Mini Kit (Omega Bio-Tek). The specific shRNA sequences used are as follows: shADAMTS9-AS1#1: GGUGUUGAACUGUGAAGA AGA; shADAMTS9-AS1#2: CCACUAAGAAAGACAACAAGG; si-ADAMTS9 CGA CAAAUGUGAUACCUUAGG; si-HuR#1: CGAGCUCAGAGGUGAUCAAAG; si-HuR#2: CGAGCUCAGAGGUGAUCAAAG.

Western blot

Whole cell lysates were prepared in RIPA buffer (Beyotime, P.R. China) containing a mixture of protease and phosphatase inhibitors. Then, equal amounts of protein lysates (40 µg) were separated on 10% SDS-PAGE gels and transferred to PVDF membranes (Millipore, MA) with cold transfer buffer. Membranes were blocked with 5% skim milk for 1 h at room temperature (RT) and then incubated with the relevant primary antibody overnight at 4 °C. Membranes were washed and subsequently incubated with secondary antibodies conjugated to horseradish peroxidase (HRP). Enhanced chemiluminescence was used to visualize proteins. Western blotting was performed with the following primary antibodies: anti-GAPDH (Sigma-Aldrich, 1:8000), anti-ADAMTS9 (Abcam, USA, 1:1000), anti-HuR (Abcam, USA, 1:1000), Goat anti-mouse IgG (HRP) and goat anti-rabbit IgG (HRP) secondary antibodies were diluted 1:2000.

RNA extraction and quantitative real-time PCR

Total RNA was extracted using TRIzol Reagent (Invitrogen, CA, USA) according to the manufacturer's protocol. One microgram of total RNA was reverse transcribed using a high-power capacity cDNA Reverse Transcriptase Kit (TOYOBO, JAPAN). Quantitative RT-PCR (qRT-PCR) was performed using SYBR Green PCR Master Mix (Invitrogen) on a Roche LightCycler 480 system (Roche Diagnostics, Germany) to determine relative expression of ADAMTS9-AS1. GAPDH was used as a housekeeping gene. The primer sequences were as follows: ADAMTS9-AS1-F: 5′-ATAGGGAACAGATGTGAGGATAGC A-3′; ADAMTS9-AS1-R: 5′- TACACTTGGAGGGCAGAGGAATGGC-3′; ADAMTS9-AS1#1-F: 5′- GTGCTCGGTGACTTCTCTGGCTTTA-3′; ADAMTS9-AS1#1-R: 5′-GGGCAGAGGAATGGCAAGAAGTAAG-3′; ADAMTS9-AS1#2-F: 5′- ACCACTAAG AAAGACAACAAGGGCT-3′; ADAMTS9-AS1#2-R: 5′- CTTCCTTCCCTATTAAGC

Zhao *et al. Cancer Nanotechnology*   (2023) 14:57

Page 20 of 24

CTTGAGA-3′; ADAMTS9-AS1#3-F: 5′- AACCACTAAGAAAGACAACAAGGGC-3′; ADAMTS9-AS1#3-R: 5′- TTCTCAGGATTTACCCACACTCTTG-3′; ADAMTS9-F: 5′- AGGATTAACCTGGCTGGTGAC-3′; ADAMTS9-R: 5′- GACTTCTACAAACCGTGG ATAGG-3′; GAPDH-F: 5′-CATGTTCGTCATGGGTGTGAA-3′; and GAPDH-R: 5′-GGC ATGGACTGTGGTCATGAG-3′

CCK-8 assays

96-well plates were seeded with 8×10^3 cells per well, with a volume of 100 μl. Ten microliters of CCK-8 (Dojindo Molecular Technologies, Inc., Kyushu, Japan) was added to each well and incubated for 2 h at 37 °C on each subsequent day. A multimode reader (Bio-Tek, USA) was used to detect absorbance at 460 nm in order to determine the effects of ADAMTS9-AS1 on cell growth and viability.

Colony formation assays

Cells were seeded in 6-well plates and cultured in medium containing 10% FBS for 2 weeks. Colonies were fixed with methanol for 30 min, and 500 μl of 0.5% crystal violet was subsequently added (Sigma-Aldrich, St. Louis, MO, USA) to each well for 30 min for visualization and counting.

Flow cytometry analysis

Flow cytometry analysis was performed according to the manufacturer's protocol. Cells were seeded in 6-well plates for 24 h, harvested and washed twice with cold PBS. Then, the cells were stained with PE-conjugated Annexin V and PI (Cat. No. 559763, BD Biosciences, San Jose, CA) for 15 min at room temperature in the dark. Finally, the cells were analyzed using a FACSCalibur flow cytometer (BD Biosciences, San Jose, CA, USA).

Xenograft study

Athymic BALB/c mice (males, 4 weeks old) were obtained from Shanghai Laboratory Animal Company (SLAC, Shanghai, China). All mice were kept in specific pathogen-free (SPF) conditions and all experiments conducted were approved by the Institutional Animal Care and Use Committee (IACUC) of Harbin Medical University, Harbin, China. Animal care was in accordance with institution guidelines. A498 cells were harvested and resuspended at a concentration of 1×10^7 cells/ml. 0.1 ml of this cell suspension was injected into the skin of the front legs. 5-Aza-dC or PBS was injected intraperitoneally. The tumor weight and sizes were measured every 4 days. 28 days after injection of cells, mice were killed, tumor sizes/weights were evaluated, and tissues were stored at −80 °C for further analysis.

Chemotherapeutics

5-Aza-dC was purchased from Sigma-Aldrich (USA) and dissolved in DMSO to obtain a 1 mmol/L stock solution. Drugs were stored at −20 °C. Chemoresistance experiments (IC50 evaluation) were performed according to a standard protocol.

RNA pull-down and mass spectrometry

Biotin-labeled ADAMTS9-AS1 was transcribed in vitro using Biotin RNA Labeling Mix (Roche, Germany) according to the manufacturer's instructions. Biotinylated RNAs were denatured for 5 min at 65 °C and slowly cooled down to room temperature. Then, the folded RNA was incubated with streptavidin magnetic beads (Thermo Fisher Scientific, Waltham, MA, USA) for 1 h at 4 °C. After washing 4×5 min with wash buffer (10 mM HEPES pH 7.0, 400 mM NaCl, 1 mM DTT, 1% Triton X-100, protease inhibitor cocktail (Roche), the protein lysate was pre-cleared by streptavidin magnetic beads and incubated with the folded RNA-beads complex for 3 h at 4 °C in the presence of yeast tRNA. After extensive washing, beads were boiled 40 μl of $1 \times$ SDS loading buffer for 10 min at 100 °C. The lncRNA-interacting proteins were further separated by sodium dodecyl sulphate–polyacrylamide gel electrophoresis and the gel was silver stained. Then, ADAMTS9-AS1 specific bands were subjected to mass spectrometry and retrieved in human proteomic library.

UV cross-linking RNA-IP (CLIP)

1×10^{7} cells were washed with cold PBS one time and cells were irradiated once with UV cross-linked at 4.00 mJ/cm². Cells were lysed in lysis buffer (50 mM Tris–HCL, pH 7.4, 100 mM NaCl, 1% NP-40, 0.1% SDS, 0.5% sodium deoxycholate, protease inhibitor cocktail and RNase inhibitors) and transferred to 1.5-mL microtubes. After the cells were pre-cleared with protein A/G sepharose beads, cell lysates were treated with indicated antibody or IgG control at 4 °C overnight. Then, the antibody–RNA complexes were collected by using the blocked Protein A/G sepharose beads. After four washes in the presence of protease inhibitor cocktail and RNase inhibitor, the immunoprecipitated RNA was eluted and isolated for the subsequent reaction to reverse transcription and using for further qRT-PCR analysis for the target RNA.

RNA–RNA interaction assay

5 pmol biotin-labeled RNAs were incubated with 2.5 pmol non-biotin-labeled RNA or cell lysate in incubation buffer (100 mM Tris pH 7.5, 25 mM NaCl and MgCl2) for 2 h at 4 °C. Following incubation, the complexes were incubated with streptavidin magnetic beads (Thermo Fisher Scientific, Waltham, MA, USA) for 2 h. After then, beads were washed six times with RIP Wash Buffer (Millipore, Cat# CS203177). Beads were digested with proteinase K buffer containing RIP Wash Buffer, 1% SDS (Millipore, Cat# CS203174), and 1.2 μg/μL proteinase K (Millipore, Cat# CS203218) at 55 °C for 30 min. After beads digestion, RNA was extracted and qRT-PCR was performed to detect relative RNA levels.

Dual-luciferase reporter assay

The promoter of ADAMTS9-AS1 segment ($- 1000 \sim +1$) or ADAMTS9 3′UTR were constructed into pGL3-control and pMIR plasmid. The plasmid was co-transfected with 50 ng Renilla luciferase reporter plasmid into cells that cultured in 24-well plates by using Lipofectamine 2000. The luciferase activities were measured using The Dual-Luciferase® Reporter Assay System (Promega, USA) after 48 h transfection.

Zhao *et al. Cancer Nanotechnology*   (2023) 14:57

Page 22 of 24

Statistical analysis

A Chi-square test was used to determine the association of clinical and pathological variables with ADAMTS9 and ADAMTS9-AS1 expression levels. Survival differences were assessed by the Kaplan–Meier method and log-rank test. The total survival time was calculated as the time from surgery to death. A Student's t-test was used to analyze differences between groups in the in vitro experiments. The Spearman correlation coefficient was calculated for correlation analysis. The data are expressed as the mean $\pm$ SEM, and all results were confirmed by at least three independent experiments. The SPSS 18.0 software system (SPSS, Chicago, IL) was used for statistical analysis. $p < 0.05$ was considered statistically significant.

Supplementary Information

The online version contains supplementary material available at https://doi.org/10.1186/s12645-023-00210-w.

Additional file 1: Figure S1. ADAMTS9-AS1 is downregulated in ccRCC and is associated with poor prognosis. (A-B). The expression levels of ADAMTS9-AS1 in pan-cancer (A) and additional cancer types (B) from the TCGA database. (C-D) Correlation between ADAMTS9-AS1 and cancer stage in pan-cancer (C) and additional cancer types (D) from the TCGA database. (E). Kaplan–Meier survival analysis of ccRCC patients with low or high expression of ADAMTS9-AS1 from TCGA database. **Figure S2.** ADAMTS9-AS1 inhibits ccRCC cell viability and sensitivity to 5-aza-dC in vitro. (A). ADAMTS9-AS1 overexpression and KD efficiency was confirmed by qRT-PCR in OS-RC-2 cells. (B-C). Cell growth was determined by CCK-8 (left) and colony formation (right) assays following ADAMTS9-AS1 overexpression (B) and KD (C) in OS-RC-2 cells. (D) Cell viability of OS-RC-2 cells were detected by CCK-8 assay following ADAMTS9-AS1 overexpression (left) or ADAMTS9-AS1 knockdown (right) and treatment with a concentration gradient of 5-aza-dC. (E) The apoptosis ratio was detected by FACS assay following ADAMTS9-AS1 overexpression (left) or ADAMTS9-AS1 knockdown (right) in OS-RC-2 cells with or without 5-aza-dC treatment. The data derived from three independent experiments are presented as mean $\pm$ SEM in the bar graphs (A-E). Controls were normalized to 1 (A-D). *P < 0.05, **P < 0.01, ***P < 0.001. **Figure S3.** ADAMTS9-AS1 is physically associated with HuR and increases the binding of HuR to ADMTS9 3'UTR. (A). The protein bound to ADAMTS9-AS1 was determined by mass spectrometry. (B). ADAMTS9-AS1 associated HuR was predicted by bioinformatics website (catRAPID). (C). The protein expression levels of HuR were measured by WB after ADAMTS9-AS1 overexpressed or KD in A498 cells. (D). ADMTS9 3'UTR associated HuR was predicted by bioinformatics website (catRAPID). **Figure S4.** The expression of ADAMTS9-AS1 in 50 pairs of ccRCC and corresponding adjacent normal tissues. The expression of ADAMTS9-AS1 in adjacent normal tissues. The expression of ADAMTS9-AS1 in ccRCC tissues. **Figure S5.** ADAMTAS9-AS1 deficiency potentiates 5Aza-induced renal tumor suppression in vivo. The representative images of xenograft tumors infected with LV-Flag or LV-ADAMTAS9-AS1. The representative images of xenograft tumors infected with control shRNA or sh-ADAMTAS9-AS1 which were treated with vehicle or 5-aza.

Author contributions
CW and XL designed the research studies and analyzed and interpreted the data. EZ, BG, TR, BY, YL, WH, and WW conducted experiments and acquired data. XL, CW and EZ drafted the manuscript, and all authors contributed revisions. All authors read and approved the final manuscript.

Data availability
The authors declare that all data supporting the findings of this study are available.

Declarations

Ethics approval and consent to participate
The use of human clinical tissues was approved by the Research Ethics Committee of Harbin Medical University, China. All mice were kept in specific pathogen-free (SPF) conditions and all experiments conducted were approved by the Institutional Animal Care and Use Committee (IACUC) of Harbin Medical University, Harbin, China.

Informed consent
Not applicable.

References

Agrawal K et al (2018) Nucleosidic DNA demethylating epigenetic drugs - A comprehensive review from discovery to clinic. Pharmacol Ther 188:45–79

Barth DA et al (2019) Current concepts of non-coding RNAs in the pathogenesis of non-clear cell renal cell carcinoma. Cancers (basel). https://doi.org/10.3390/cancers11101580

Beermann J et al (2016) Non-coding RNAs in development and disease: background, mechanisms, and therapeutic approaches. Physiol Rev 96(4):1297–1325

Capitanio U et al (2019) Epidemiology of renal cell carcinoma. Eur Urol 75(1):74–84

Chen LL (2016) Linking long noncoding RNA localization and function. Trends Biochem Sci 41(9):761–772

Chen L et al (2017) ADAMTS9 is silenced by epigenetic disruption in colorectal cancer and inhibits cell growth and metastasis by regulating Akt/p53 signaling. Cell Physiol Biochem 44(4):1370–1380

Chen W et al (2020) LncRNA ADAMTS9-AS1, as prognostic marker, promotes cell proliferation and EMT in colorectal cancer. Hum Cell 33(4):1133–1141

de Cubas AA, Rathmell WK (2018) Epigenetic modifiers: activities in renal cell carcinoma. Nat Rev Urol 15(10):599–614

Dragomir MP et al (2020) Non-coding RNAs in GI cancers: from cancer hallmarks to clinical utility. Gut 69(4):748–763

Du W et al (2013) ADAMTS9 is a functional tumor suppressor through inhibiting AKT/mTOR pathway and associated with poor survival in gastric cancer. Oncogene 32(28):3319–3328

Dubail J, Apte SS (2015) Insights on ADAMTS proteases and ADAMTS-like proteins from mammalian genetics. Matrix Biol 44–46:24–37

Fang S, Zhao Y, Hu X (2020) LncRNA ADAMTS9-AS1 restrains the aggressive traits of breast carcinoma cells via sponging miR-513a-5p. Cancer Manag Res 12:10693–10703

Flippot R et al (2019) Long non-coding RNAs in genitourinary malignancies: a whole new world. Nat Rev Urol 16(8):484–504

George S, Rini BI, Hammers HJ (2019) Emerging role of combination immunotherapy in the first-line treatment of advanced renal cell carcinoma: a review. JAMA Oncol 5(3):411–421

Hao K et al (2019) LncRNA-Safe contributes to cardiac fibrosis through Safe-Sfrp2-HuR complex in mouse myocardial infarction. Theranostics 9(24):7282–7297

Hsieh JJ et al (2017) Renal cell carcinoma. Nat Rev Dis Primers 3:17009

Huarte M (2015) The emerging role of lncRNAs in cancer. Nat Med 21(11):1253–1261

Jonasch E, Gao J, Rathmell WK (2014) Renal cell carcinoma. BMJ 349:g4797

Kopp F, Mendell JT (2018) Functional classification and experimental dissection of long noncoding RNAs. Cell 172(3):393–407

Larkin J et al (2012) Epigenetic regulation in RCC: opportunities for therapeutic intervention? Nat Rev Urol 9(3):147–155

Li N et al (2020) Long non-coding RNA ADAMTS9-AS1 suppresses colorectal cancer by inhibiting the Wnt/β-catenin signalling pathway and is a potential diagnostic biomarker. J Cell Mol Med 24(19):11318–11329

Lin C, Yang L (2018) Long noncoding RNA in cancer: wiring signaling circuitry. Trends Cell Biol 28(4):287–301

Lo PH et al (2007) Identification of a tumor suppressive critical region mapping to 3p142 in esophageal squamous cell carcinoma and studies of a candidate tumor suppressor gene, ADAMTS9. Oncogene 26(1):148–157

Lung HL et al (2008) Characterization of a novel epigenetically-silenced, growth-suppressive gene, ADAMTS9, and its association with lymph node metastases in nasopharyngeal carcinoma. Int J Cancer 123(2):401–408

Maher ER (2013) Genomics and epigenomics of renal cell carcinoma. Semin Cancer Biol 23(1):10–17

Marconi L et al (2016) Systematic review and meta-analysis of diagnostic accuracy of percutaneous renal tumour biopsy. Eur Urol 69(4):660–673

McLysaght A, Hurst LD (2016) Open questions in the study of de novo genes: what, how and why. Nat Rev Genet 17(9):567–578

Nikolaou M et al (2018) The challenge of drug resistance in cancer treatment: a current overview. Clin Exp Metastasis 35(4):309–318

Palazzo AF, Koonin EV (2020) Functional long non-coding RNAs evolve from junk transcripts. Cell 183(5):1151–1161

Peng L et al (2013) Epigenetic inactivation of ADAMTS9 via promoter methylation in multiple myeloma. Mol Med Rep 7(3):1055–1061

Posadas EM, Limvorasak S, Figlin RA (2017) Targeted therapies for renal cell carcinoma. Nat Rev Nephrol 13(8):496–511

Ricketts CJ et al (2016) SnapShot: renal cell carcinoma. Cancer Cell 29(4):610–610

Schmitt AM, Chang HY (2016) Long noncoding RNAs in cancer pathways. Cancer Cell 29(4):452–463

Shao B et al (2018) The 3p14.2 tumour suppressor ADAMTS9 is inactivated by promoter CpG methylation and inhibits tumour cell growth in breast cancer. J Cell Mol Med 22(2):1257–1271

Shuch B et al (2015) Understanding pathologic variants of renal cell carcinoma: distilling therapeutic opportunities from biologic complexity. Eur Urol 67(1):85–97

Slack FJ, Chinnaiyan AM (2019) The role of non-coding RNAs in oncology. Cell 179(5):1033–1055

van der Mijn JC et al (2014) Predictive biomarkers in renal cell cancer: insights in drug resistance mechanisms. Drug Resist Updat 17(4–6):77–88

Wan J et al (2019) Data mining and expression analysis of differential lncRNA ADAMTS9-AS1 in prostate cancer. Front Genet 10:1377

Wang KC, Chang HY (2011) Molecular mechanisms of long noncoding RNAs. Mol Cell 43(6):904–914

Wang X et al (2019a) UDP-glucose accelerates SNAI1 mRNA decay and impairs lung cancer metastasis. Nature 571(7763):127–131

Wang A et al (2019b) Long noncoding RNA EGFR-AS1 promotes cell growth and metastasis via affecting HuR mediated mRNA stability of EGFR in renal cancer. Cell Death Dis 10(3):154

Yan P et al (2017) Cis- and trans-acting lncRNAs in pluripotency and reprogramming. Curr Opin Genet Dev 46:170–178

Yao RW, Wang Y, Chen LL (2019) Cellular functions of long noncoding RNAs. Nat Cell Biol 21(5):542–551

Yoon JH et al (2012) LincRNA-p21 suppresses target mRNA translation. Mol Cell 47(4):648–655

Zhang C et al (2010) High-resolution melting analysis of ADAMTS9 methylation levels in gastric, colorectal, and pancreatic cancers. Cancer Genet Cytogenet 196(1):38–44

Znaor A et al (2015) International variations and trends in renal cell carcinoma incidence and mortality. Eur Urol 67(3):519–530

Publisher's Note